International Journal of GEOMATE, April, 2025 Vol.28, Issue 128, pp.68-75
ISSN: 2186-2982 (P), 2186-2990 (O), Japan, DOI: https://doi.org/10.21660/2025.128.g14167
Geotechnique, Construction Materials and Environment

PREDICTION OF LONG-TERM CREEP BEHAVIOR OF AN HDPE GEOGRID BY ACCELERATED STRESS RELAXATION TECHNIQUES

*Rawiwan Eakintumas[1] and Warat Kongkitkul[2]

[1,2] Department of Civil Engineering, Faculty of Engineering, King Mongkut's University of Technology Thonburi, Bangkok, Thailand

*Corresponding Author, Received: 20 Nov. 2024, Revised: 20 Jan. 2025, Accepted: 22 Jan. 2025

ABSTRACT: Accurately understanding the creep behavior of polymer geosynthetic reinforcements is key to designing durable geosynthetic-reinforced soil (GRS) structures. Establishing the creep reduction factor (RF_{CR}) for a specific design life has traditionally required extended conventional creep testing to produce a creep rupture curve. To expedite this process, temperature-acceleration techniques, such as the conventional time-temperature superposition (TTS) and the stepped isothermal method (SIM), have been adopted to accelerate creep deformation. Since the material's viscous properties influence both creep and stress relaxation, stress relaxation occurs at a faster rate than creep for the same irreversible strain under a given load. A framework has been empirically developed to relate the time history of stress relaxation to creep strain, allowing for effective prediction of long-term creep strain using short-term stress relaxation data. This study applies temperature-acceleration methods to short-term creep and stress relaxation tests on a high-density polyethylene (HDPE) geogrid. Results provide extended time histories for creep strain and stress relaxation, with durations extended by a factor of 250. By establishing a relationship between these time histories, a comprehensive method to predict long-term creep behavior is developed, combining the time factors of both methods to produce an approximately 1,635-fold extension. This streamlined approach enables an efficient and reliable prediction of HDPE geogrid creep behavior over long durations.

Keywords: Stress relaxation, Creep, Temperature, Geogrid, HDPE

1. INTRODUCTION

Geosynthetic reinforcements are widely used in soil structures, providing cost-effective and high-performance solutions for engineering projects like roads, embankments, and retaining walls. Numerous studies have demonstrated that geosynthetic reinforcements enhance the shear strength and deformation properties of soil, thereby increasing its bearing capacity. These improvements directly relate to the stabilization features essential for geosynthetic-reinforced soil (GRS) structures [1, 2]. Additionally, a critical aspect of geosynthetic reinforcements that warrants attention is their creep behavior.

Understanding the creep (CP) behavior of polymer geosynthetic reinforcement is crucial for evaluating the long-term performance of GRS structures, where the creep reduction factor (RF_{CR}) is used in the design process [3]. While the conventional creep tests are reliable, they are time-consuming. To speed up the testing process, two accelerated methods are often employed: the conventional time-temperature superposition (TTS) and the stepped isothermal method (SIM) [4]. The TTS method predicts long-term creep behavior by using short-term creep data obtained at different temperatures, which are shifted along the time axis to create a master curve based on a reference temperature. In the SIM test, the temperature is increased step by step, with each step held constant for a period before moving to the next. This approach accelerates the creep rate, and similar to TTS, a master curve is developed. Due to its efficiency, SIM is widely adopted in the industry.

A recent study [5] demonstrated that creep (CP) behavior can be inferred from stress relaxation (SR) behavior. Under the same initial tensile load, the time required to reach an equivalent irreversible strain rate for SR (Δt_{SR}) is shorter than that for CP (Δt_{CP}), and the irreversible strain increment from SR ($\Delta\varepsilon_{SR}^{ir}$) is smaller than that of CP ($\Delta\varepsilon_{CP}^{ir}$). By establishing relationships between Δt_{SR} and Δt_{CP}, and between $\Delta\varepsilon_{SR}^{ir}$ and $\Delta\varepsilon_{CP}^{ir}$ for the same irreversible strain rates, the CP strain history can be predicted from the SR load history. The study showed that, based on a 3-hour SR test, the predicted Δt_{CP} values were longer than Δt_{SR} values by factors of 3.07 for polypropylene (PP) and 6.29 for high-density polyethylene (HDPE) geogrids [5].

A recent approach has effectively combined TTS and SIM techniques for PP geogrids [6]. These methods accelerated short-term SR and CP tests to obtain long-term equivalent histories. This framework predicted the Δt_{CP} to be 29 times longer than the SR test time using TTS (SR-TTS) [6]. However, despite its success in extending the prediction of creep duration, it slightly underestimated the final CP behavior compared to the results from long-term CP tests.

This study enhances understanding of the long-term behavior of HDPE geogrids by advancing a

combined technique that uses short-term SR-TTS and CP-SIM tests to predict creep strain history from stress relaxation load history. By applying Achereiner's method [7] to develop master curves, the research establishes a novel framework that effectively correlates Δt_{SR} and Δt_{CP}, and $\Delta \varepsilon_{SR}^{ir}$ and $\Delta \varepsilon_{CP}^{ir}$ scenarios. This significantly reduces the time and resources required for long-term testing. This methodology holds significant value in the design of geotechnical structures.

2. RESEARCH SIGNIFICANCE

This study addresses the challenge of evaluating the long-term creep behavior of geosynthetic reinforcements. By integrating temperature-accelerated stress relaxation (SR-TTS) and creep testing (CP-SIM), this framework enables accurate predictions of extended long-term creep behavior. Instead of relying solely on CP-SIM to determine creep-rupture curves, the combined use of CP-SIM and SR-TTS provides a more reliable and efficient approach. This method is applicable to geosynthetic reinforcements, particularly the widely used HDPE geogrid, enhancing the design and performance of geosynthetic-reinforced soil (GRS) structures under sustained loads.

3. METHODOLOGY

3.1 Test Material and Test Conditions

A uniaxial HDPE geogrid was used in this study, characterized by a long-elliptical shape with dimensions of 220 mm in the longitudinal direction and 16 mm in the transverse direction. It has a maximum tensile strength (V_{ult}) of 90 kN/m and a glass transition temperature of -125°C [8]. A reference temperature of 30°C was chosen to represent ambient conditions in Thailand. The sustained loading during CP was set at 40 kN/m, approximately 44% of V_{ult}. The initial tensile load for SR was also set at 40 kN/m. The duration of each test at various temperatures followed the guidelines specified in ASTM D6992 [9]

3.2 Test Apparatus and Measuring Devices

A special temperature-controlled tensile loading apparatus (Fig. 1) was used. It consists of: i) tensioning unit; and ii) heating unit. The tensioning unit applies tension to a specimen using roller-clamps and a double-action air-cylinder, with internal air pressure regulated by a computer via an electro-pneumatic transducer. The heating unit generates and circulates hot air within an insulated test chamber, with air entering from the bottom, distributing evenly, and exiting from the top. Half of the air is released, while the other half is mixed with room temperature air and recirculated. Two thermocouples monitor the system: one at the heater for overtemperature protection and another inside the chamber to regulate its temperature via an independent control unit.

The tensile load was measured by an axial load cell outside the chamber, with a heat insulator preventing heat transfer. A three-strand specimen was pretensioned, and two edge strands were cut to form a single-strand specimen (Fig. 1). A displacement transducer on a miniature frame measured axial deformation for tensile strain calculations. Additionally, a thermocouple was used to monitor the temperature inside the chamber.

3.3 Test Programs

This study employed various tensile loading-temperature schemes, using SIM and TTS techniques to accelerate CP strain and SR load relief.

3.3.1 Monotonic loading-constant temperature (ML-CT)

The specimen was tensioned with a controlled small pretension load at room temperature. The temperature, *T* was then increased to specified values and held constant. Then, continuous monotonic loading (ML) was applied at a rate of 0.6 kN/m/min.

3.3.2 Creep with SIM

The specimen was pretensioned at room temperature, then *T* was increased to 30°C. The tensile load (*V*) is increased to 40 kN/m at a rate of 0.6 kN/m/min and then held constant. During this period, *T* was held constant for four stages, each lasting four hours. At the end of each stage, *T* was immediately increased by 7°C. Therefore, CP was performed at *T* = 30°C, 37°C, 44°C, and 51°C using a single specimen via CP-SIM.

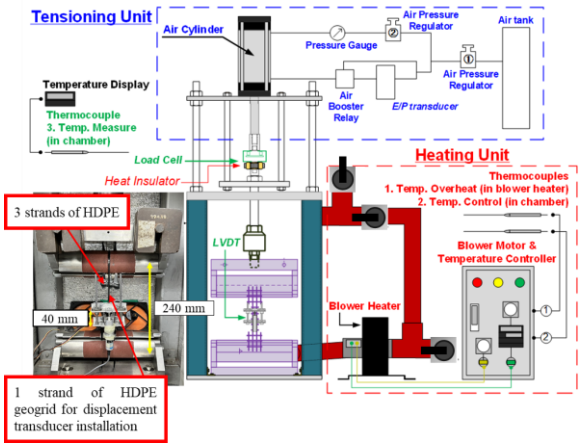

Fig. 1 Schematic of the test apparatus used in the study (modified from Kongkitkul et al. [10])

3.3.3 Stress Relaxation with TTS

First, tensile strain values corresponding to V = 40 kN/m for different T values from ML-CT test results were determined as target tensile strains. The specimen was pretensioned at room temperature, then T is increased to either 30°C, 37°C, 44°C, or 51°C and held constant. V was then increased at a rate of 0.6 kN/m/min until the target tensile strain is achieved. The tensile strain was then controlled constant using a computer with feedback from the current measured tensile strain. For SR-TTS, four specimens were tested each at T = 30°C, 37°C, 44°C, and 51°C. Note that the SIM technique could not be successfully applied to the SR test due to the difficulty in maintaining constant strain during the 7°C increase steps.

4. TEST RESULTS AND DISCUSSION

4.1 Tensile Load-Strain Relations

The relationships between tensile load (V) and tensile strain (ε) obtained from the CP-SIM and SR-TTS tests are presented in Fig. 2. In the CP-SIM and SR-TTS tests, the ML was conducted before the start of CP or SR, using a load rate of 0.6 kN/m/min. Four temperature stages of 30°C, 37°C, 44°C, and 51°C were used to accelerate creep in the CP-SIM test and were similarly applied to the SR-TTS test. The duration for each temperature stage in the CP-SIM and SR-TTS tests was 240 minutes.

The tensile load-strain relationships observed in the CP-SIM test during the ML phase, before the initiation of CP, showed similarities to that obtained in the SR-TTS test at 30°C. In the CP-SIM test, it was evident that as creep progressed under a constant load of 40 kN/m, the strain (ε) steadily increased. In the SR-TTS test, the stress relaxation was controlled to maintain a constant tensile strain of 4.38% during the relaxation period.

This strain level remained consistent across all four tests conducted at different temperatures (30°C, 37°C, 44°C, and 51°C), demonstrating that higher temperatures result in a reduction in the initial tensile load at the start of SR. This reduction underscores the impact of temperature increases on the load-strain-time behavior of geosynthetic reinforcements [11, 12]. Furthermore, Fig. 2 shows that the initial points at the start of both the CP and SR stages at T = 30°C are nearly identical, indicating the high quality of the test results.

4.2 Master Creep Curve from CP-SIM Test

Fig. 3 shows the time histories of creep strain (ε_{CP}) and temperature (T) from the CP-SIM test. In this figure, ε_{CP} is defined as zero when V is zero. While T is held constant, ε_{CP} increases with time at a decreasing rate. When T is stepped up to the next value, ε_{CP} accelerates and then increases again at a decreasing rate. The analysis of the CP-SIM test begins with the determination of the virtual start time, t', as illustrated in Fig. 3. t' represents the time required for completing thermal expansion between the current stage's temperature and T = 30°C, with V maintained at zero [7].

Next, the relationships between ε_{CP} and the dwell time (t-t') for different temperature values are plotted, with dwell time represented on a log scale, as shown in Fig. 4. The raw data from the CP-SIM test correspond to a series of independent creep curves, which can be combined into a smooth master creep curve through horizontal shifting, owing to the continuous creep deformation observed in the CP-SIM data. The horizontal shifting factor, α_T, is defined as the ratio of the time required for a viscoelastic process to occur at any given temperature, T to the time required for the same process at the reference temperature, T_1, as shown in Equation 1.

$$\varepsilon\left(T_1, t\right) = \varepsilon\left(T, \frac{t}{\alpha_T}\right) \tag{1}$$

The Williams-Landel-Ferry (WLF) equation (Equation 2) is typically used to determine α_T [13].

$$\log\left(\alpha_T\right) = \frac{-C_1\left(T - T_1\right)}{C_2 + T - T_1} \tag{2}$$

where C_1 and C_2 are empirical constants. For temperatures between the glass transition temperature, T_g, and T_g + 43K, C_1 and C_2 are usually 8.86 and 101.6, respectively, and are known as universal constants [14]. However, for the HDPE geogrid tested in this study, with T_g = −125°C and T_1 = 30°C, these constants were adjusted to C_1= 17.72 and C_2 = 101.6 through trial and error. This method assumes that the constants C_1 and C_2 are applicable across all temperature steps. Table 1 lists the α_T values as per respective T.

When T is higher than T_1, the time required to reach the same strain value at T is shorter than at T = T_1 by a factor of α_T. Consequently, α_T values are positive and less than unity, resulting in a negative $\log(\alpha_T)$ values, as shown in Table 1. The ε_{CP} vs. $\log_{10}(t\text{-}t')$ segments for T higher than T_1 are horizontally shifted to the right along the log(time) axis and overlapped to form a single smooth, continuous curve (Fig. 4). The data are then vertically shifted downward to account for deformation caused by thermal expansion during sample heating, ensuring a smooth transition in the ε_{CP} vs. $\log_{10}(t\text{-}t')$ segment for the subsequent temperature. This adjustment helps maintain a continuous master creep curve, as shown in Fig. 4.

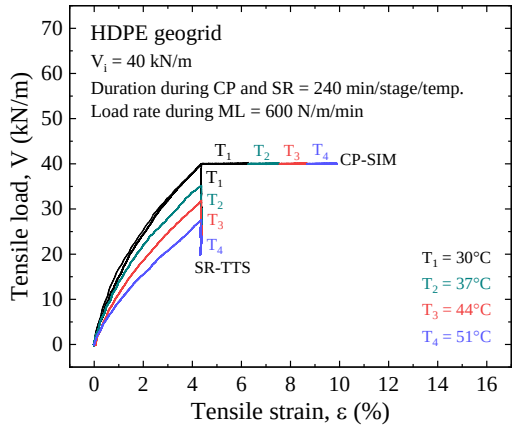

Fig. 2 Tensile load-strain relationships from CP-SIM and SR-TTS tests performed in the present study

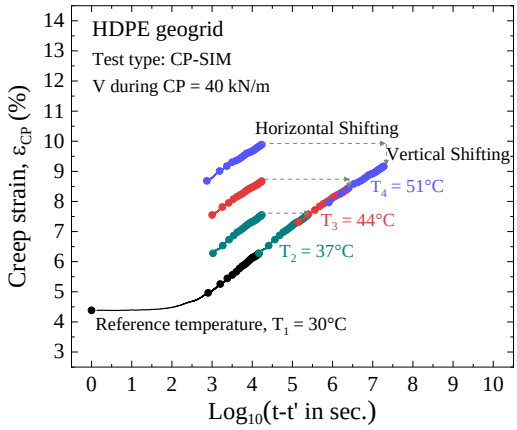

Fig. 4 Master creep curve production for CP-SIM test at V = 40 kN/m and T_1 = 30°C

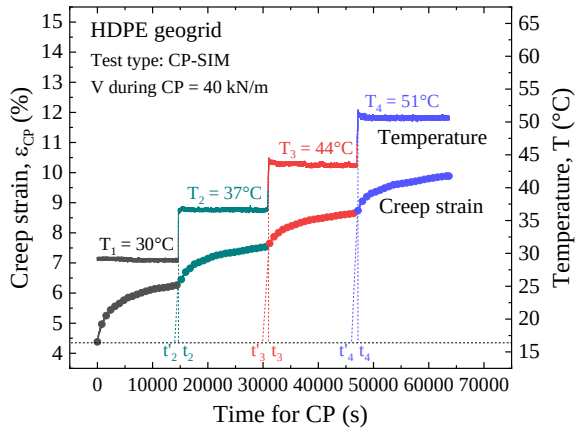

Fig. 3 Time histories of creep strain and temperature during CP-SIM test at V = 40 kN/m.

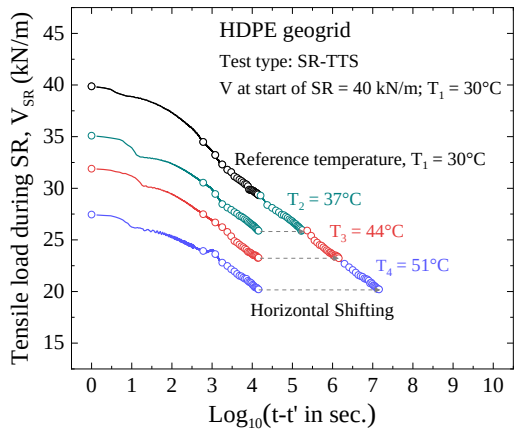

Fig. 5 Master stress relaxation curve production for SR-TTS test at V_i = 40 kN/m at T_1 = 30°C

Table 1 Horizontal shifting factors (α_T)

Reference temperature, T_1 (°C)	Elevated temperature, T (°C)	Horizontal shifting factor α_T	$\log(\alpha_T)$
30	37	7.211×10^{-2}	-1.142
	44	7.145×10^{-3}	-2.146
	51	9.226×10^{-4}	-3.035

4.3 Master Stress Relaxation Curve from SR-TTS Test

From an ML-CT test performed at T = 30°C, when V = 40 kN/m, the corresponding strain (ε) is 4.38%. The SR-TTS tests were conducted at different temperatures by tensioning the specimen until ε = 4.38% and then keeping the strain constant. Fig. 5 shows the time histories of V during SR (V_{SR}) from the SR-TTS tests at different temperatures. In these plots, the V values at the starting points (V_i) correspond to ε = 4.38% for different T, so the V_i for different T are not the same and decrease with increasing T. When V first equals V_i, time t' is defined. The time scale is plotted as $\log_{10}(t\text{-}t')$, considering only the time increment during SR.

Next, the initial nonlinear portions of the V_{SR} - $\log_{10}(t\text{-}t')$ curves for temperatures higher than 30°C were trimmed, and then they were shifted horizontally to the right along the log(time) axis. This process is similar to the procedures used for the CP-SIM test and employs the WLF equation with the same C_1 and C_2 values. In the SR-TTS test, vertical shifting was not necessary as the curves after horizontal shifting were smooth. The master stress relaxation curve obtained is shown in Fig. 5.

Horizontal and vertical shifts significantly influence the accuracy of master creep and stress relaxation curves. Verification through conventional long-term creep and stress relaxation tests is crucial, but it is beyond the scope of this paper.

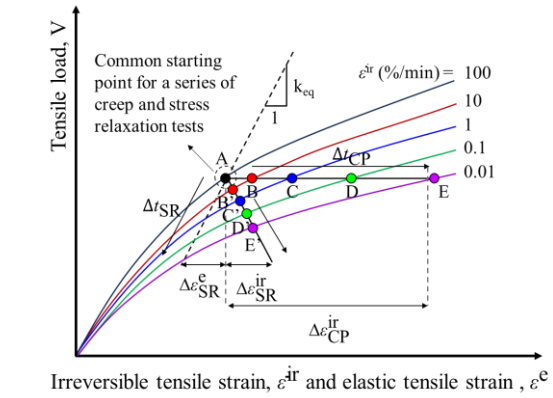

(a)

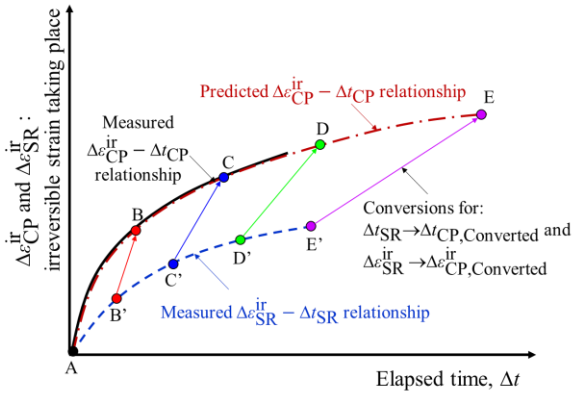

(b)

Fig. 6 Concepts of predicting CP from SR for isotach viscosity: (a) (V - ε^{ir}) relationships with CP and SR stages; and (b) prediction of time history of CP strain from SR.

4.4 Concepts of Stress Relaxation-to-Creep Prediction

CP and SR of polymer geosynthetic reinforcements are known to be responses governed by their viscous properties [3, 15], which allows these behaviors to be linked. Nuntapanich et al. [5] proposed a framework to predict CP behavior from SR behavior. Their concepts can be summarized as follows.

Fig. 6(a) shows the schematic relationships between V and irreversible strain (ε^{ir}) by monotonic loading (ML) at different irreversible strain rates ($\dot{\varepsilon}^{ir}$) for polymer geosynthetic reinforcements exhibiting the isotach property. Suppose that CP and SR tests are performed immediately after ML reaches point A, making point A the starting point for both CP and SR. Points B, C, D, and E represent the (V, ε^{ir}) states during CP where ($\dot{\varepsilon}^{ir}$) decreases successively. Similarly, points B', C', D', and E' represent the states during SR for the same respective $\dot{\varepsilon}^{ir}$. Thus, points B&B', C&C', D&D', and E&E' correspond to the same $\dot{\varepsilon}^{ir}$.

Along these corresponding (V, ε^{ir}) stages for CP and SR, the time for creep (Δt_{CP}) and the irreversible strain increment during creep ($\Delta\varepsilon^{ir}_{CP}$), as well as the time for stress relaxation (Δt_{SR}) and the irreversible strain increment during stress relaxation ($\Delta\varepsilon^{ir}_{SR}$), can be determined. Relationships between Δt_{CP} and Δt_{SR} and between $\Delta\varepsilon^{ir}_{CP}$ and $\Delta\varepsilon^{ir}_{SR}$ can then be developed. Consequently, for a given V, the time history of creep strain can be predicted from the time history of SR for V_i equal to V in the CP test, based on these relationships.

Fig. 6(b) illustrates the $\Delta\varepsilon^{ir}_{CP} - \Delta t_{CP}$ relationship predicted from the measured $\Delta\varepsilon^{ir}_{SR} - \Delta t_{SR}$ using the described concept. Since SR occurs significantly faster than CP, the predicted Δt_{CP} is substantially longer than the Δt_{SR} spent in the experiment.

4.5 Development of Prediction Framework

According to the nonlinear three-component model [16, 17], total strain increment ($\Delta\varepsilon$) consists of the elastic ($\Delta\varepsilon^{e}$) and irreversible ($\Delta\varepsilon^{ir}$) components as shown in Equation 3.

$$\Delta\varepsilon = \Delta\varepsilon^{e} + \Delta\varepsilon^{ir} \tag{3}$$

During creep, V is constant, or $\Delta V = 0$, and thus the elastic strain increment during CP, $\Delta\varepsilon^{e}_{CP}$, is zero. As per Equation 3, it means that during creep, $\Delta\varepsilon$ is always equal to $\Delta\varepsilon^{ir}$ ($\Delta\varepsilon_{CP} = \Delta\varepsilon^{ir}_{CP}$). From the experiment, the time history of $\Delta\varepsilon = \Delta\varepsilon_{CP} = \Delta\varepsilon^{ir}_{CP}$ can be plotted. Then, the time history of the irreversible strain rate during creep ($\dot{\varepsilon}^{ir}_{CP}$) can be determined by differentiating $\Delta\varepsilon^{ir}_{CP}$ to time during creep (Δt_{CP}). Fig. 7(a) shows the relationship between $\dot{\varepsilon}^{ir}_{CP}$ and Δt_{CP} in full-logarithm scale.

On the other hand, during the SR test, V decreases, resulting in a negative elastic strain increment ($\Delta\varepsilon^{e}_{SR}$), which can be determined from the decrease of V during SR, ΔV, by Equation 4.

$$\Delta\varepsilon^{e}_{SR} = \Delta V / k_{eq}(V) \tag{4}$$

where $k_{ep}(V)$ is the tensile load-dependent equivalent elastic stiffness. In this study, the value of $k_{ep}(V)$ for the HDPE geogrid was assumed to be constant and equal to 1,484 kN/m. This value is consistent with the one assumed for HDPE geogrid in the study by Nuntapanich et al. [5].

During the SR test, $\Delta\varepsilon$ is kept zero, and therefore, to satisfy Equation 3, a positive irreversible strain increment ($\Delta\varepsilon^{ir}_{SR}$) develops ($\Delta\varepsilon^{ir}_{SR} = -\Delta\varepsilon^{e}_{SR}$) By performing SR, the time history of ΔV can be measured, and it can be converted to the time history of $\Delta\varepsilon^{e}_{SR}$ with Equation 4, and finally to the time history

of $\Delta\varepsilon_{SR}^{ir}$. Then, similar to CP, the time history of the irreversible strain rate during SR ($\Delta\dot{\varepsilon}_{SR}^{ir}$) can be determined by differentiating $\Delta\varepsilon_{SR}^{ir}$with respect to time during SR (Δt_{SR}). Fig. 7(b) shows the relationship between $\Delta\dot{\varepsilon}_{SR}^{ir}$ and Δt_{SR}in full-logarithm scale.

In addition, the irreversible strain increment during creep ($\Delta\varepsilon_{CP}^{ir}$) and during stress relaxation ($\Delta\varepsilon_{SR}^{ir}$) corresponding to Δt_{CP} and Δt_{SR} can be realized by the CP and SR experiments, respectively. The $\dot{\varepsilon}_{CP}^{ir}$ vs. $\Delta\varepsilon_{CP}^{ir}$ and $\dot{\varepsilon}_{SR}^{ir}$ vs. $\Delta\varepsilon_{SR}^{ir}$ relationships can be plotted in full-logarithm scale, as shown in Figs. 8(a) and 8(b), respectively.

A set of preselected $\dot{\varepsilon}_{SR}^{ir}$ values of 10^{-4}, 2×10^{-5}, 5×10^{-6}, and 10^{-6} %/s were projected to $\dot{\varepsilon}_{CP}^{ir}$ vs. Δt_{CP} and $\dot{\varepsilon}_{SR}^{ir}$ vs. Δt_{SR} relationships to read the corresponding Δt_{CP} and Δt_{SR}, respectively (Fig. 7). These preselected $\dot{\varepsilon}_{SR}^{ir}$ values were also projected to $\dot{\varepsilon}_{CP}^{ir}$ vs. $\Delta\varepsilon_{CP}^{ir}$ and $\dot{\varepsilon}_{SR}^{ir}$ vs. $\Delta\varepsilon_{SR}^{ir}$ relationships to read the corresponding $\Delta\varepsilon_{CP}^{ir}$ and $\Delta\varepsilon_{SR}^{ir}$, respectively (Fig. 8).

The Δt_{CP} and Δt_{SR} values corresponding to the same preselected $\dot{\varepsilon}^{ir}$ values can be plotted together and presented in a full-logarithm scale as shown in Fig. 9. Similarly, $\Delta\varepsilon_{CP}^{ir}$ and $\Delta\varepsilon_{SR}^{ir}$ values corresponding to the same preselected $\dot{\varepsilon}^{ir}$ values can be plotted together and presented in a full-logarithm scale as shown in Fig. 10. Both Δt_{CP} vs. Δt_{SR} and $\Delta\varepsilon_{CP}^{ir}$ vs. $\Delta\varepsilon_{SR}^{ir}$ relationships are essentially linear in full-logarithm scale and located above the line of equality. This means that to reach the same $\dot{\varepsilon}^{ir}$, Δt_{CP} is significantly longer than Δt_{SR} and $\Delta\varepsilon_{CP}^{ir}$ is significantly larger than $\Delta\varepsilon_{SR}^{ir}$. Data points in Figs. 9 and 10 can be fitted with Equations 5 and 6, respectively

$$\log(\Delta t_{CP}) = S_t.\log(\Delta t_{SR}) + \log(\Delta t_0) \quad (5)$$

$$\log(\Delta\varepsilon_{CP}^{ir}) = S_\varepsilon.\log(\Delta\varepsilon_{SR}^{ir}) + \log(\Delta\varepsilon_0) \quad (6)$$

where S_t and S_ε are the slopes of Δt_{CP} vs. Δt_{SR} and $\Delta\varepsilon_{CP}^{ir}$ vs. $\Delta\varepsilon_{SR}^{ir}$ relationships presented in Figs. 9 and 10, respectively; Δt_0 is the value of Δt_{CP} when Δt_{SR} = 1.0 second; and $\Delta\varepsilon_0$ is $\Delta\varepsilon_{CP}^{ir}$ when $\Delta\varepsilon_{SR}^{ir}$ = 1.0%

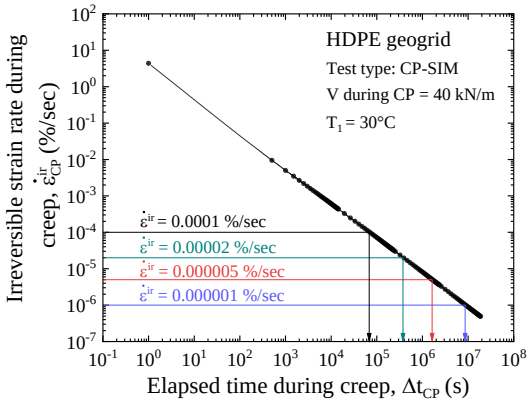

(a)

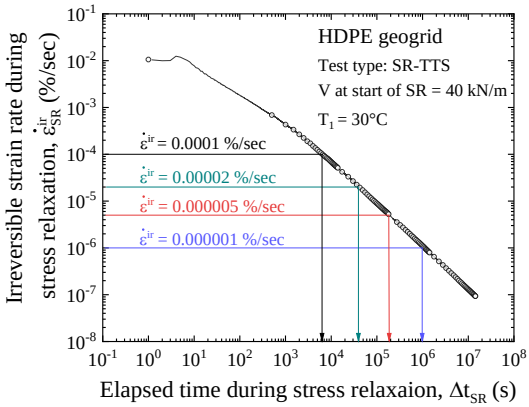

(b)

Fig. 7 Relationships between irreversible strain rate and time: (a) $\dot{\varepsilon}_{CP}^{ir}$ vs. Δt_{CP} from CP-SIM test; and (b) $\dot{\varepsilon}_{SR}^{ir}$ vs. Δt_{SR} from SR-TTS test

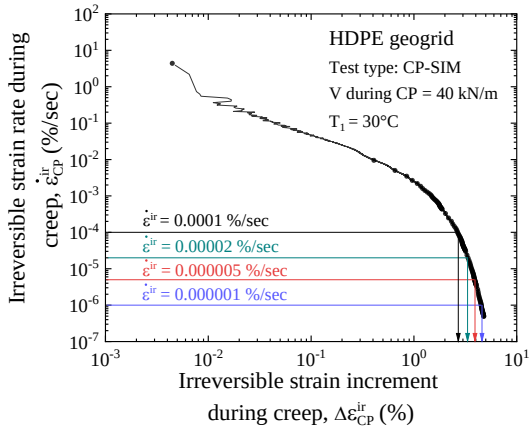

(a)

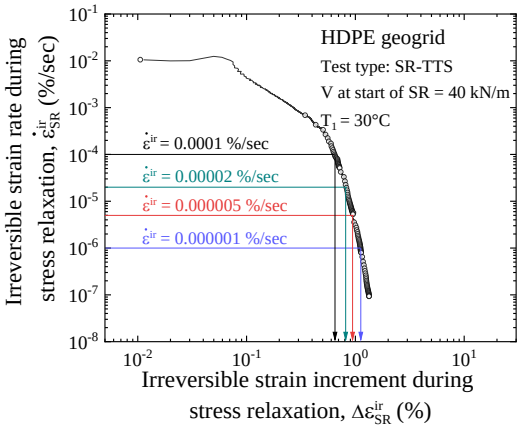

(b)

Fig. 8 Relationships between irreversible strain rate and irreversible strain increment: (a) $\dot{\varepsilon}_{CP}^{ir}$ vs. $\Delta\varepsilon_{SR}^{ir}$ from CP-SIM test; and (b) $\dot{\varepsilon}_{SR}^{ir}$ vs. $\Delta\varepsilon_{SR}^{ir}$ from SR-TTS test

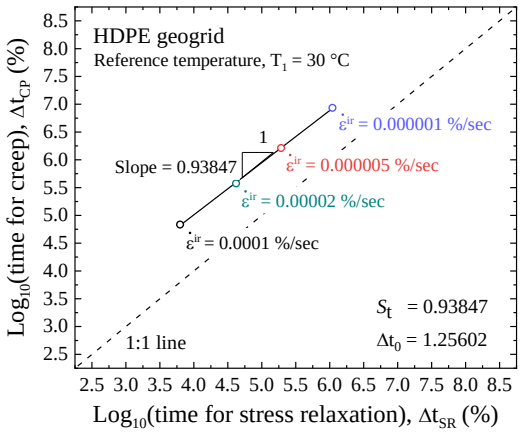

Fig. 9 Δt_{CP} vs. Δt_{SR} relationship

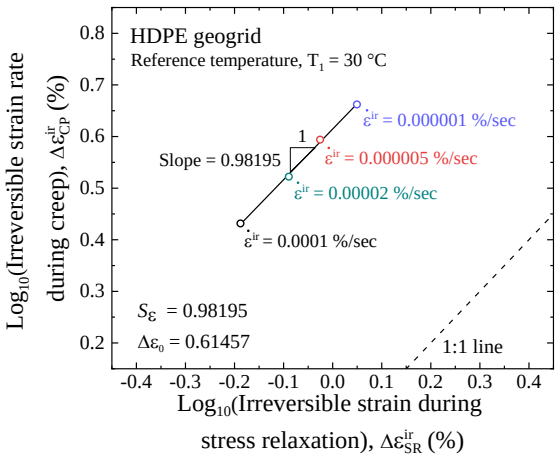

Fig. 10 $\Delta \varepsilon_{CP}^{ir}$ vs. $\Delta \varepsilon_{SR}^{ir}$ relationship

4.6 Prediction of Time History of Creep from SR-TTS

Both CP-SIM and SR-TTS tests implemented four temperature stages, each lasting for four hours, resulting in a total duration of 16 hours. By using increasing temperature to accelerate creep strain and load decrease during SR, a master creep curve and a master stress relaxation curve were obtained, as shown in Figs. 4 and 5, respectively. The time was extended to around 4,000 hours. By re-zeroing the creep strain value at the start of creep on the master creep curve in Fig. 4, the $\Delta \varepsilon_{CP}^{ir}$ vs. Δt_{CP} can be plotted in an arithmetic scale, as shown in Fig. 11. Similarly, by re-zeroing the load at the start of SR on the master stress relaxation curve in Fig. 5, $\Delta \varepsilon_{SR}^{ir}$ can be determined using Equation 4, and then the $\Delta \varepsilon_{SR}^{ir}$ vs. Δt_{SR} can be plotted in an arithmetic scale, as shown in Fig. 11. At a time of 4,000 hours, $\Delta \varepsilon_{CP}^{ir}$ is significantly larger than $\Delta \varepsilon_{SR}^{ir}$.

From the $\Delta \varepsilon_{SR}^{ir}$ vs. Δt_{SR} obtained from the SR-TTS test, the Δt_{CP} can be predicted by substituting Δt_{SR} into Equation 5, and the $\Delta \varepsilon_{CP}^{ir}$ by substituting $\Delta \varepsilon_{SR}^{ir}$ into Equation 6. Fig. 11 also shows the $\Delta \varepsilon_{CP}^{ir}$ vs. Δt_{CP} predicted as described above. It can be seen that the predicted creep strain at a time of 4,000 hours is very accurate, and more importantly, the ending time by the prediction was extended from 4,000 hours to 26,161 hours, an extension factor of 6.540.

In conclusion, the time required for an SR-TTS test is 16 hours, which results in a master stress relaxation curve effective for 4,000 hours. The master stress relaxation curve can be used to predict the time history of creep strain by the stress relaxation-to-creep prediction framework effective for 26,161 hours. Notably, the final predicted creep period (26,161 hours) is significantly longer than the actual test duration (16 hours), showing a 1,635-fold increase.

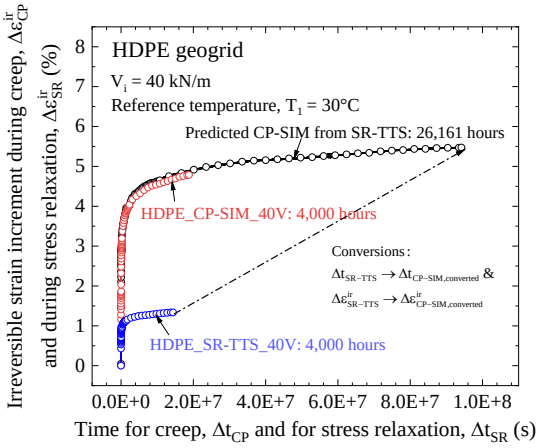

Fig. 11 Time history of irreversible strain: comparison among SR-TTS test, CP-SIM test, and predicted value

5. CONCLUSIONS

In this study, temperature-accelerated creep tests using the SIM technique (CP-SIM) and temperature-accelerated stress relaxation tests using the TTS technique (SR-TTS) were performed on an HDPE geogrid to obtain master creep and master stress relaxation curves, respectively. These two master curves were used to construct a stress relaxation (SR)-to-creep (CP) prediction framework via the link based on the irreversible strain rate with the nonlinear three-component (NTC) model. The following findings were obtained:

– The master creep and stress relaxation curves obtained from CP-SIM and SR-TTS, respectively, lasted for a total time of 16 hours each (i.e., 4 hours per temperature for 4 temperatures), prolonging to an extended time of 4,000 hours. In other words, time can be extended by a factor of 250 using the temperature-acceleration technique.

- An SR-to-CP prediction framework developed based on the NTC model linked via irreversible strain rate was successfully developed. The master creep curve can be well predicted by the master stress relaxation curve, and more importantly, time can be extended from 4,000 hours to 26,161 hours, increased by a factor of 6.540.
- Combining both techniques, the actual experimental time of 16 hours can be extended to 26,161 hours, increased by a factor of 1,635.

6. ACKNOWLEDGMENTS

The authors would like to express gratitude to King Mongkut's University of Technology Thonburi (KMUTT) for financial support through The Petchra Pra Jom Klao Ph.D. scholarship under contract Grant No. 3/2565, and to Tencate Geosynthetics (Thailand) Co., Ltd. for providing geogrids for this study.

7. REFERENCES

[1] Tulebekova A., Zhankina A., Imambayeva R., Makhiyev B., Khapin A., and Anop D., A practical solution for improving soil bases in problematic engineering conditions, International Journal of GEOMATE, Vol. 25, No.108, 2023, pp. 191-198.

[2] Tulebekova A., Kusbergenova Z., Dosmukhambetova B., Bakirova D., Tleulenova G., and Zhumadilov I., Effects of geogrid and non-woven geotextiles on the shear behavior of soil, International Journal of GEOMATE, Vol. 27, No.123, 2024, pp. 75-82.

[3] Hirakawa D., Kongkitkul W., Tatsuoka F., and Uchimura T., Time-dependent stress–strain behaviour due to viscous properties of geogrid reinforcement, Geosynthetics International, Vol. 10, No.6, 2003, pp. 176-199.

[4] Thornton J., Paulson J., and Sandri D. Conventional and stepped isothermal methods for characterizing long term creep strength of polyester geogrids, Conference proceedings, in Proceedings 6th International Conference on Geosynthetics, Atlanta. 1998, pp. 691-698.

[5] Nuntapanich N., Kongkitkul W., Tatsuoka F., and Jongpradist P., Prediction of creep behaviour from load relaxation behaviour of polymer geogrids, Geosynthetics International, Vol. 25, No.3, 2018, pp. 334-349.

[6] Eakintumas R., and Kongkitkul, W., Predicting the creep behavior of polypropylene geogrid using temperature-accelerated stress relaxation test results, Conference proceedings, in Proceeding of the 21st Southeast Asian Geotechnical Conference and 4th AGSSEA Conference, 2023.

[7] Achereiner F., Engelsing K., Bastian M., and Heidemeyer P., Accelerated creep testing of polymers using the stepped isothermal method, Polymer Testing, Vol. 32, No.3, 2013, pp. 447-454.

[8] Al-Barqawi M., Aqel R., Wayne M., Titi H., and Elhajjar R., Polymer geogrids: a review of material, design and structure relationships, Materials, Vol. 14, No.16, 2021, p. 4745.

[9] ASTM D6992, Standard test method for accelerated tensile creep and creep-rupture of geosynthetic materials based on time-temperature superposition using the stepped isothermal method, 2009, ASTM International: West Conshohocken, Pennsylvania.

[10] Kongkitkul W., Tabsombut W., Jaturapitakkul C., and Tatsuoka F., Effects of temperature on the rupture strength and elastic stiffness of geogrids, Geosynthetics International, Vol. 19, No.2, 2012, pp. 106-123.

[11] Chantachot T., Kongkitkul W., and Tatsuoka F., Load-strain-time behaviours of two polymer geogrids affected by temperature, International Journal of GEOMATE, Vol. 10, No.21, 2016, pp. 1869-1876.

[12] Chantachot T., Kongkitkul W., and Tatsuoka F., Effects of temperature on elastic stiffness of a HDPE geogrid and its model simulation, International Journal of GEOMATE, Vol. 12, No.32, 2017, pp. 94-100.

[13] Ferry J.D., Viscoelastic properties of polymers, John Wiley & Sons, 1980.

[14] Van Krevelen D.W. and Te Nijenhuis K., Properties of polymers: their correlation with chemical structure; their numerical estimation and prediction from additive group contributions, Elsevier, 2009.

[15] Kongkitkul W., Hirakawa D., Tatsuoka F., and Uchimura T., Viscous deformation of geosynthetic reinforcement under cyclic loading conditions and its model simulation, Geosynthetics International, Vol. 11, No.2, 2004, pp. 73-99.

[16] Di Benedetto H., Tatsuoka F., and Ishihara M., Time-dependent shear deformation characteristics of sand and their constitutive modelling, Soils and Foundations, Vol. 42, No.2, 2002, pp. 1-22.

[17] Tatsuoka F., Ishihara M., DI B.H., and Kuwano R., Time-dependent shear deformation characteristics of geomaterials and their simulation, Soils and Foundations, Vol. 42, No.2, 2002, pp. 103-129.